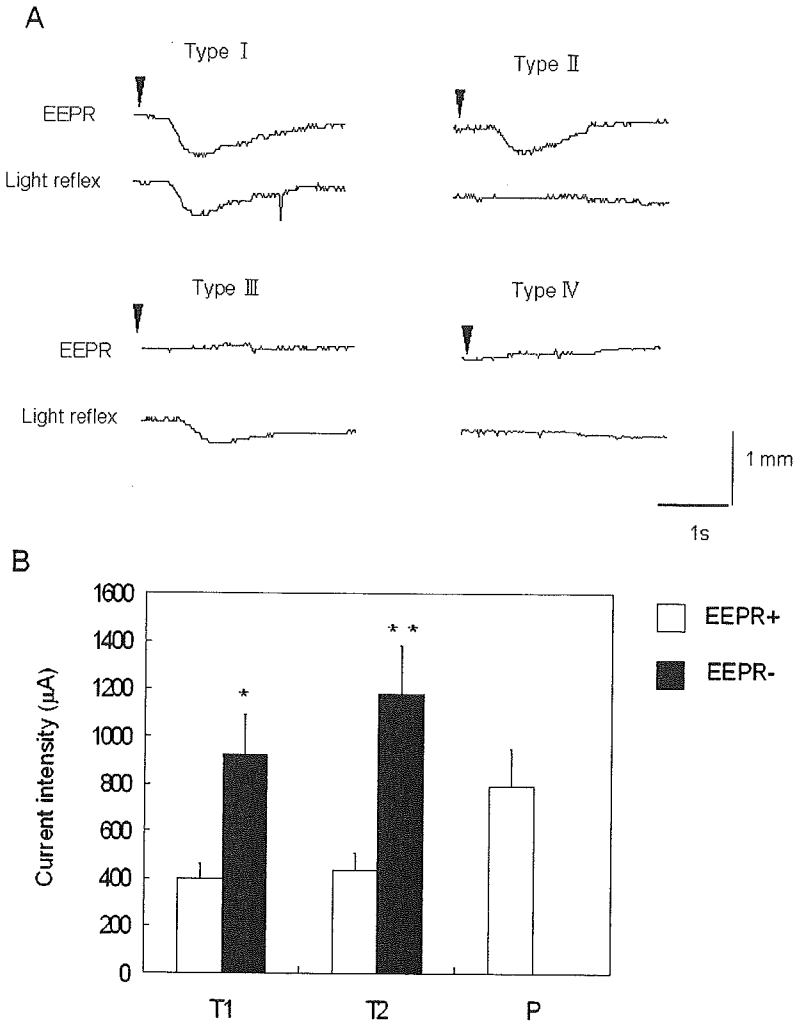

Fig. 6 **a**. Four types recordings of EEPR and light reflex from RP patients. Type I light reflex (+) and EEPR (+), type II light reflex (−) and EEPR (+), type III light reflex (+) and EEPR (−), and type IV light reflex (−) and EEPR (−). *Arrow head* indicates the onset of stimulation.
b. Comparison of thresholds in RP patients with an EEPR (type I and type II) with RP patients without an EEPR (type III and type IV) There were significant differences between patients with an EEPR and without an EEPR (student *t*-test: T1; **P*<0.05, T2; ***P*<0.01)

We also found that the threshold of phosphenes and logMAR visual acuity were not significantly correlated. The thresholds of blind patients were lower than those of some patients who were not blind (Fig. 3). These findings indicate that threshold of phosphenes rather than the visual acuity may be a better indicator of the residual RGC function in patients with severe retinal degeneration.

We further compared the thresholds in the group with a preservation of the central visual field left to those with a preservation of the peripheral visual field. Although the mean T1 threshold in the central visual field group was higher than that in peripheral visual field group, the mean T2 threshold in the central visual field group was not lower but higher than that in peripheral visual field group in spite of the remaining of the center of visual field (Fig. 4). Thus, the RGCs in the central retina were preserved more in the peripheral visual field group than in the central visual field group.

The mean current intensity of T1 and T2 in CRD patients was lower than those in RP patients (Fig. 5e), suggesting that the RGC function were more preserved in CRD patients than in RP patients in both the macula and extramacular areas.

Although all CRD patients showed a positive EEPRs, all RP patients did not show them. Moreover thresholds of phosphenes varied among RP patients. There were significant differences between the T1 and T2 for the group with an EEPR and those without an EEPR (Fig. 6). The presence or absence of EEPR is a good indicator of the extent of residual RGC function in patients with retinal degeneration.

On the contrary, the mean threshold of EEPR was twice as high as that of T2 in the group with an EEPR, although the thresholds of T2 and EEPR were close in normal subjects. Thus the thresholds of EEPR would not be a good indicator of the central phosphene in RP patients. A certain number of RGCs may have to be functioning to evoke a

pupillary constriction. However, in advanced RP patients, the density of RGC is so low that a higher current is needed to depolarize the widely scattered RGCs to evoke a pupillary constriction, while phosphene may be perceived even if a small number of RGCs were depolarized by TES.

These data suggest that three parameters, T1, T2 and P, measured by TES examination can be used to select candidates for retinal prostheses.

In summary, we have developed a safe method to elicit phosphenes and EEPR by TES to study the residual RGC function in patients with retinal degeneration. In RP patients, the presence of EEPR did not necessarily indicate the preservation of RGCs in the central retina, but reflected the overall activity of residual RGCs. Therefore, our method may provide information on the function of residual RGC which cannot be examined with currently available ophthalmologic instruments. Thus, among several tests required to select candidates for a retinal prosthesis [35],TES may have an important role.

Acknowledgements The authors thank Yozo Miyake, Satoshi Suzuki, Mineo Kondo and Yutaka Fukuda for advice and discussions.

References

1. Brindley GS (1955) The site of electrical excitation of the human eye. J Physiol 127:189–200
2. Chow AY, Chow VY (1997) Subretinal electrical stimulation of the rabbit retina. Neurosci Lett 225:13–16
3. Chow AY, Chow VY, Packo KH, Pollack JS, Peyman GA, Schuchard R (2004) The artificial silicon retina microchip for the treatment of vision loss from retinitis pigmentosa. Arch Ophthalmol 122:460–469
4. Delbeke J,Pins D, Michaux G, Wanet-Defalque MC, Parrini S, Veraart C (2001)Electrical stimulation of anterior visual pathways in retinitis pigmentosa. Invest Ophthalmol Vis Sci 42:291–297
5. Fariss RN, Li ZY, Milam AH (2000) Abnormalities in rod photoreceptors, amacrine cells, and horizontal cells in human retinas with retinitis pigmentosa. Am J Ophthalmol 129:215–223
6. Gebhard JW (1952) Thresholds of the human eye for electric stimulation by different wave forms. J Exp Psychol 44:132–140
7. Haruta M, Kosaka M, Kanegae Y, Saito I, Inoue T, Kageyama R, Nishida A, Honda Y, Takahashi M (2001) Induction of photoreceptor-specific phenotypes in adult mammalian iris tissue. Nat Neurosci 4:1163–1164
8. Hesse L, Schanze T, Wilms M, Eger M (2000) Implantation of retina stimulation electrodes and recording of electrical stimulation responses in the visual cortex of the cat. Graefe's Arch Clin Exp Ophthalmol 238:840–845
9. Humayun MS, Price M, de Juan Jr E, Barron Y, Moskowitz M, Klock IB, Milam AH (1999) Morphometric analysis of the extramacular retina from postmortem eyes with retinitis pigmentosa. Invest Ophthalmol Vis Sci 40:143–148
10. Humayun MS, Weiland JD, Fujii GY, Greenberg RJ, Williamson R, Little J, Mech B, Climmarusti V, Van Boemel G, Dagnelie G, de Juan Jr E (2003) Visual perception in a blind subject with a chronic microelectronic retinal prosthesis. Vision Res 43:2573–2581
11. Jensen RJ, Rizzo JF 3rd, Ziv OR, Grumet A, Wyatt J (2003) Thresholds for activation of rabbit retinal ganglion cells with an ultrafine, extracellular microelectrode. Invest Ophthalmol Vis Sci 44:3533–3543
12. Johnson LN, Guy ME, Krohel GB, Madsen RW (2000) Levodopa may improve vision loss in recent-onset, nonarteritic anterior ischemic optic neuropathy. Ophthalmology 107: 521–526
13. Kanda H, Morimoto T, Fujikado T, Tano Y, Fukuda Y, Sawai H (2004) Electrophysiological studies on the feasibility of suprachoroidal-transretinal stimulation for artificial vision in normal and RCS rat. Invest Ophthalmol Vis Sci 45:560–566
14. Kawasumi M (1985) Distribution of current intensities inside the electrically stimulated eye. Nippon Ganka Gakkai Zasshi 89:766–772
15. Li ZY, Kjavin IJ, Milam AH. (1995) Rod photoreceptor neurite sprouting in retinitis pigmentosa. J Neurosci 15:5429–5438
16. Majji AB, Humayun MS, Weiland JD, Suzuki S, D'Anna SA, de Juan Jr E (1999) Long-term histological and electrophysiological results of an inactive epiretinal electrode array implantation in dogs. Invest Ophthalmol Vis Sci 40:2073–2081
17. Margalit E, Maia M, Weiland JD, Greenberg RJ, Fujii GY, Torres G, Piyathaisere DV, O'Hearn TM, Liu W, Lazzi G, Dangnelie G, Scribner DA, de Juan Jr E, Humayun MS (2002) Retinal prosthesis for the blind. Surv Ophthalmol 47:335–356
18. Marmor MF, Aguirre G, Arden G (1983) Retinitis pigmentosa: a symposium on terminology and methods of examination. Ophthalmology 90: 126–131
19. Motokawa K, Iwama K (1950) Resonance in electrical stimulation of the eye. Tohoku J. Exp Med 53:201–206
20. Motokawa K, Ebe M (1952) Selective stimulation of color receptors with alternating currents. Science 25:115:92–94
21. Miyake Y, Yanagida K, Yagasaki K (1980) Clinical application of EER (electrically evoked response). (1) Analysis of EER in normal subjects. Nippon Ganka Gakkai Zasshi 84: 354–360
22. Miyake Y, Yanagida K, Yagasaki K (1980) Clinical application of EER (electrically evoked response) (2) Analysis of EER in patients with dysfunctional rod or cone visual pathway. Nippon Ganka Gakkai Zasshi 84:502–509

23. Pagon RA (1988) Retinitis pigmentosa. Surv Ophthalmol 33:137–177
24. Potts AM, Inoue J (1968) The electrically evoked response of the visual system (EER). Invest Ophthalmol 7:269–278
25. Potts AM, Inoue J (1969) The electrically evoked response of the visual system (EER) II. Effect of adaptation and retinitis pigmentosa. Invest Ophthalmol 8:605–613
26. Rizzo JF 3rd, Wyatt J, Loewenstein J, Kelly S, Shire D (2003) Perceptual efficacy of electrical stimulation of human retina with a microelectrode array during short-term surgical trials. Invest Ophthalmol Vis Sci 44: 5362–5369
27. Santos A, Humayun MS, de Juan E Jr, Greenberg RJ, Marsh MJ, Klock IB, Milam AH (1997) Preservation of the inner retina in retinitis pigmentosa: a morphometric analysis. Arch Ophthalmol 115:511–515
28. Schwahn HN, Gekeler F, Kohler K, Kobuch K, Sachs HG, Schulmeyer F, Jacob W, Gabel VP, Zrenner E (2001) Studies on the feasibility of a subretinal visual prosthesis: data from Yucatan micropig and rabbit. Graefe's Arch Clin Exp Ophthalmol 239:961–967
29. Stone JL, Barlow WE, Humayun MS, de Juan E Jr, Milam AH (1992) Morphometric analysis of macular photoreceptors and ganglion cells in retinas with retinitis pigmentosa. Arch Ophthalmol 110:1634–1639
30. Tanino T, Kato S, Kawasumi M (1981) Studies on electrically evoked pupillary reflex-Indirect reflex and its frequency characteristics. Jpn J Ophthalmol 25:423–429
31. Tanino T, Kurihara K (1982) Electrically evoked direct and consensual reflexs of the pupil. Jpn J Ophthalmol 26:462–467
32. Tanino T. (1982) Studies on electrically evoked pupillary reaction 1. Indirect electrical reaction and its frequency characteristic. Nippon Ganka Gakkai Zasshi (Japanese) 61:397–402
33. Veraart C, Raftopoulos C, Mortimer JT, Delbeke J, Pins D, Michaux G, Vanlierde A, Parrini S, Wanet-Defalque MC (1998) Visual sensations produced by optic nerve stimulation using an implanted self-sizing spiral cuff electrode. Brain Res 813:181–186
34. Walter P, Heimann K (2000) Evoked cortical potentials after electrical stimulation of the inner retina in rabbits. Graefe's Arch Clin Exp Ophthalmol 238:315–318
35. Yanai D, Lakhanpal RR, Weiland JD, Mahadevappa M, Van Boemel G, Fujii G, Greenberg R, Caffey S, de Juan Jr E (2003) The value of preoperative tests in the selection of blind patients for a permanent microelectronic implant. Trans Am Ophthalmol Soc 101: 223–230
36. Young MJ, Ray J, Whiteley RS, Klassen H, Gage FH (2000) Neuronal differentiation and morphological integration of hippocampal progenitor cells transplanted to the retina of immature and mature dystrophic rats. Mol Cell Neurosci 16:197–205

Graefe's Arch Clin Exp Ophthalmol
(2006) 244: 364–375

LABORATORY INVESTIGATION

DOI 10.1007/s00417-005-0073-9

Xiaoyun Fang
Hirokazu Sakaguchi
Takashi Fujikado
Makoto Osanai
Yasushi Ikuno
Motohiro Kamei
Masahito Ohji
Tetsuya Yagi
Yasuo Tano

Electrophysiological and histological studies of chronically implanted intrapapillary microelectrodes in rabbit eyes

Received: 10 November 2004
Revised: 13 May 2005
Accepted: 17 May 2005
Published online: 4 August 2005

X. Fang (✉) · H. Sakaguchi · Y. Ikuno · M. Kamei · M. Ohji · Y. Tano
Department of Ophthalmology E-7,
Graduate School of Medicine,
Osaka University,
2-2 Yamadaoka,
Suita, Osaka, 565-0871, Japan
e-mail: fangxyp@hotmail.com
Tel.: +81-6-68793456
Fax: +81-6-68793458

T. Fujikado
Department of Visual Science,
Osaka University,
Graduate School of Medicine,
Suita, Osaka, Japan

M. Osanai · T. Yagi
Department of Electrical Engineering,
Osaka University,
Suita, Osaka, Japan

Abstract *Purpose:* To determine the safety and efficacy of transsclerally placed intrapapillary wire microelectrodes implanted chronically into the optic nerve head of rabbit eyes. *Methods:* Four platinum wire microelectrodes were passed through the sclera and implanted into the optic nerve head of five rabbit eyes for 4–6 months. Color fundus photography, fluorescein angiography, electroretinograms (ERGs), and visually evoked potentials (VEPs) were used to monitor the retina. Electrically evoked potentials (EEPs) were elicited by bipolar electrical stimulation of the optic nerve axons by different combinations of the four electrodes immediately after the implantation and at 1-month intervals thereafter. The effects of the chronic implantation of the electrodes on the morphology of the optic nerve were evaluated by histological and immunohistochemical examinations at 4 and 6 months after the implantation. *Results:* All of the electrodes remained stable in the implanted sites throughout the post-implantation period, except for one electrode that had pulled out of the optic nerve head at 1 month after implantation. No intraocular infection, inflammation, or vitreoretinal proliferation was observed in any eye. EEPs could be elicited from each pair of electrodes at all testing times. The mean threshold currents (charge densities) to evoke EEPs increased from 19.3±9.2 μA (6.0±2.9 μC/cm^2) on the implantation day to 78.8±31.9 μA (24.6±10.0 μC/cm^2) at 1 month after implantation, but did not change significantly thereafter. The implicit time and amplitude of the a- and b-waves of the ERGs and of P1 of the VEPs did not change significantly throughout the post-implantation period. Histological evaluation of the optic nerve head revealed slight tissue encapsulations surrounding the electrode and increased expression of glial fibrillary acidic protein near the surface of the optic nerve. *Conclusions:* Implantation of transscleral intrapapillary microelectrodes appears to be safe and effective. These findings indicate that the implantation of microelectrodes in the optic nerve head should be considered for an optic nerve-based prosthesis.

Keywords Electrically evoked potential · Electrical stimulation · Electrode · Optic nerve head · Histology · Visual prosthesis

Introduction

A visual prosthesis that can restore some useful vision to blind patients suffering from outer retinal degenerative diseases such as retinitis pigmentosa or age-related macular degeneration has been actively investigated over the past decade. One type of visual prosthesis is based on electrically stimulating different levels of the visual pathway, e.g., the retina, optic nerve and visual cortex, by means of implanted multi-electrode arrays to activate visual neurons [7, 8, 10, 11, 13, 14, 16, 18, 24, 26–28, 30, 33–36]. Although data have been obtained from animal and human experiments, a considerable amount of research is still necessary before the electrode arrays can be used routinely in patients.

The successful electrical stimulation of the optic nerve axons by a cuff electrode [8, 33, 34] encouraged us to search for a better method for stimulating the optic axons as part of our project to develop an optic nerve-based prosthesis. Studies of electrical microstimulation of the central nerve system and peripheral nerves have shown that penetrating electrodes have advantages over cuff-like surface electrodes [3–5, 15, 25]. We believe the optic nerve head is advantageous as an implantation site because of its anatomy and surgical accessibility. We have therefore conducted a series of experiments to determine whether multiple microelectrodes implanted into the optic nerve head can be used for electrical stimulation of optic nerve axons.

The results of our acute experiments showed that transscleral wire microelectrodes implanted into the optic nerve head of rabbit eyes can elicit cortical potentials [10, 27]. In a continuation of those experiments, we left the implanted wire microelectrodes in the optic disc for 4 and 6 months in five rabbit eyes. We evaluated the effectiveness and safety of these procedures by electrophysiological and histological means.

Materials and methods

Five Japanese albino rabbits (Hokusetsu, Setsu, Osaka, Japan), weighing 2.0–2.5 kg, were used. All experiments were performed in accordance with the Association for Research in Vision and Ophthalmology Statement for the Use of Animals in Ophthalmic and Vision Research and the policies in the Guide to the Care and Use of Laboratory Animals issued by the National Institutes of Health.

Surgical procedures

In five rabbits one eye was used for the electrode implantation, and the untouched fellow eye was used as the control. Rabbits were anesthetized with an intramuscular injection of ketamine hydrochloride (32 mg/kg body weight) and xylazine hydrochloride (4 mg/kg body weight).

Epoxy-insulated, 50-μm-diameter platinum wires (Unique Medical, Tokyo, Japan) with approximately 500 μm of the tip exposed were used as stimulating electrodes. The implantation technique was approximately the same as described [10], except for the fixation of the extraocular segment of the electrodes. Vitrectomy was not performed prior to electrode implantation. Briefly, four scleral paracenteses were made 1.5–2 mm posterior to the limbus in the four quadrants with a 30-gauge needle. Four wire electrodes were carefully passed through the four holes into the vitreous cavity. The exposed tips of the wire electrodes were grasped with an intraocular microforceps and the tips were inserted into the optic disc in the four quadrants to a depth of about 1.0 mm. Care was taken to avoid the blood vessels on the optic nerve head during the implantation.

The extraocular segment of each electrode was curved against the sclera and anchored at several points to the sclera with 8-0 Vicryl sutures. The extraocular parts of the electrodes were collected and kept under the conjunctiva, and were passed through the upper eyelid. Antibiotic ointment was applied at the end of the surgery.

Two screw-type stainless steel electrodes, coated with silver, were screwed into the skull to contact the dura mater over both the left and right visual cortex 8 mm anterior to the lambdoid suture and 7 mm lateral to the midline. These served as the recording electrodes. The reference electrode was placed on the midline 15–20 mm anterior to the lambdoid suture. Both recording and reference electrodes were fixed to the skull and sealed with quick self-curing acrylic resin and the other ends were passed through the skin of the head.

Rabbits were examined before and at 1-month intervals after the implantation. Two rabbits were killed at 4 months and the remaining three at 6 months after the implantation.

Ophthalmologic examination and fluorescein angiography

Ophthalmologic examinations were performed with an operating microscope and indirect ophthalmoscopy on the operation day and at 1-month intervals after implantation. Fluorescein angiography (FA) was performed at 4 months (two eyes) and 6 months (three eyes) after implantation. Color fundus photographs were taken and FA was carried out with a Topcon TRC-50 FT retinal camera (Tokyo Optical, Tokyo, Japan). A bolus of 0.2 ml of 10% sodium fluorescein solution was injected intravenously for the FA.

Electroretinograms

Retinal function was assessed by means of full-field, dark-adapted electroretinograms (ERGs; Neuropack 2, Model MEB-7202: Nihon Kohden, Tokyo, Japan). ERGs were

recorded before, and at 1-month intervals after the implantation. The rabbits were anesthetized and pupils dilated, and a contact lens electrode (Kyoto Contact lens, Kyoto, Japan) was placed on the cornea anesthetized with 0.4% oxybuprocaine hydrochloride. After 30 min of dark adaptation, full-field ERGs were recorded from the implanted eye and the untreated fellow eye separately. The untreated eye was covered during the recordings from the implanted eye. The flash stimuli from a stroboscopic unit (LS-704B: Nihon Kohden) were controlled by a stimulator (SLS-3100: Nihon Kohden). The strobe unit was placed 15 cm in front of the rabbit's eye, the energy of the light was set at 20 J, and the stimulus duration was 1 ms. At each recording session, three separate ERGs were recorded at 1-min intervals. Each ERG consisted of a summation of 10 single sweeps at 0.1 Hz, and it was displayed on a digital storage oscilloscope (Neuropack 2, MEB-7202: Nihon Kohden). The three summated ERGs were averaged for the analyses. The mean a- and b-wave implicit times and amplitudes of the ERGs from the implanted eye were analyzed and compared with those from the untreated control eye at each time point. The a- and b-wave implicit times and amplitudes were expressed as relative values, i.e., the values in the experimental eye as percentages of those in the control eye. The averaged recordings of the control eye at each time point were taken as 100%.

Visually evoked potentials

Visually evoked potentials (VEPs) were recorded on the day of the implantation and at 1-month intervals after implantation. All VEP recording sessions were performed in the dark. The rabbits were anesthetized and the pupils were dilated as described above. Rabbits were placed on a metal plate that was connected to ground. Cortical responses were recorded between the contralateral cortical electrode and the reference electrode in response to flash stimuli to the implanted or untreated fellow eye separately. The untreated eye was covered during the first examination of the implanted eye. The rate of the flash stimuli from the stroboscopic unit (LS-704B: Nihon Kohden) was controlled by a stimulator (SLS-3100: Nihon Kohden). The strobe unit was placed 15 cm in front of the rabbit's eye, the energy of the light was set at 1.2 J, and the stimulus duration was 1 ms. At each recording session, three separate VEPs were recorded at 1-min intervals. Each VEP was the summation of 50 single responses at 1 Hz, and these were averaged and displayed on a digital storage oscilloscope (Neuropack 2, MEB-7202: Nihon Kohden). The VEP used for the analyses was the average for each eye at each time point. The means of the implicit times and amplitudes of the major positive deflection (P1) from the implanted eye were analyzed and compared with those from the untreated control eye at each time point. The mean implicit times and amplitudes of P1 from the implanted eye were expressed relative to those of the control eye. The averaged recording of the control eye at each time point was taken as 100%.

Electrically evoked potentials

Electrically evoked potentials (EEPs) were recorded on the day of implantation and at 1-month intervals after implantation. The extraocular ends of the different electrode pairs were connected to a stimulus isolation unit (SIU-A365: World Precision Instruments, Sarasota, FL) of a stimulator (SEN-7203: Nihon Kohden).

Bipolar electrical pulses were delivered to six different pairs of the four electrodes. Biphasic, current-balanced rectangular pulses with an initial cathodic pulse were used. The pulse duration was 0.25 ms, and 50 cortical responses elicited at 1 Hz were averaged for each pair of electrodes and displayed on a digital storage oscilloscope. The current necessary to elicit a cortical response was evaluated for each pair of electrodes. The current threshold was defined as that current which elicited a just-detectable peak that developed into the major positive peak of the EEP at higher currents. Generally, the EEP recordings were started at a current of 100 μA during the examination on the operation day and 300 μA during each of the follow-up examination sessions to define the major positive peak of the cortical responses. The current was then reduced gradually in 25- to 50-μA steps. If the threshold was lower than 50 μA, current steps of 5–10 μA were used. The current thresholds of EEPs from all combinations of the electrodes were averaged and used for the analyses of the mean current threshold of the EEPs for each eye.

The charge density threshold was calculated by dividing the charge per phase by the exposed surface area of the electrodes as described [10]. The exposed surface of the electrodes that were used in the present study was approximately 8.05×10^{-4} cm^2.

Scanning electron microscopy

The intravitreal segment of the implanted electrodes was cut off from the enucleated eyes at 6 months after implantation and evaluated by scanning electron microscopy (SEM). Some of the electrodes were prepared for SEM directly after removal from the eyes, and others were prepared for SEM after cleaning. The electrodes were coated with platinum before examination with the SEM (Model S-800: Hitachi, Tokyo, Japan).

Histological and immunohistochemical studies

Histological and immunohistochemical evaluations were conducted at 4 months (two eyes) and at 6 months (three eyes) to assess the effect of the microelectrodes on the histology of the optic nerve fibers. Rabbits were killed by an overdose of pentobarbital after the final stimulation session, and the experimental and control fellow eyes were immediately enucleated and fixed in 4% paraformaldehyde. The connective tissue surrounding the retrobulbar part of the optic nerve was carefully dissected to examine the position of the electrode tips macroscopically. Then, routine paraffin sections of the optic nerve head including the implanted sites were made and stained by hematoxylin-eosin for light microscopy as described [10].

Glial fibrillary acidic protein (GFAP) staining was used to evaluate the gliotic changes induced by the electrodes. For GFAP staining, longitudinal sections including the implant sites were incubated with mouse anti-GFAP monoclonal antibody (1:200; Chemicon International, Temecula, CA) overnight at 4°C. After rinsing in 0.1 M PBS, the sections were incubated with fluorescein isothiocyanate (FITC)-conjugated affinity-purified donkey anti-mouse IgG (Jackson ImmunoResearch, West Grove, PA) for 1 h at 37°C. They were then examined with an epifluorescence microscope (Zeiss, Tokyo, Japan). The selected images were digitized using a CCD camera (AxioCam: Carl Zeiss Japan, Tokyo, Japan), and the images were processed with AxioVision 2.0 software (Carl Zeiss Japan) on a Windows-based computer. Staining for the negative controls was performed simultaneously with the experimental sections. The negative controls were stained with purified mouse IgG1 (1:400; Chemicon International).

Statistical analyses

Paired and unpaired sample *t*-tests were used to determine the significance of the differences in ERGs, VEPs, and EEPs. A value of $P<0.05$ was considered statistically significant.

Results

Ophthalmoscopy and fluorescein angiography

The anterior segment remained normal and no lens opacity developed in the five eyes throughout the experimental period. No infection and dehiscence were observed in the conjunctival cul-de-sac in any eyes. There was minor bleeding from the exit site of one electrode in one rabbit that was resorbed within 1 month.

All but one of the transscleral intrapapillary wire electrodes remained quiet with the tips in the original implanted positions of the optic disc. In one eye, one of the four electrodes was displaced from the optic disc into the vitreous cavity at 1 month after implantation. No inflammation, visible vitreoretinal proliferation, retinal detachment, gliosis around the electrodes, or visible structural degradation of the wire electrodes was observed ophthalmoscopically throughout the post-implantation period in any of the eyes (Fig. 1a).

The appearance of the optic nerve head was the same as that observed preoperatively except in one eye in which a mild distortion of the optic nerve head was observed. Post-implantation fluorescein angiograms showed normal vascular perfusion in the optic nerve head, and vascular leakage of fluorescein was not observed on the optic disc in any of the eyes (Fig. 1b).

Electroretinograms

ERGs were elicited by stimulating the implanted and untreated control eyes of each of the rabbits separately before and at 1-month intervals after implantation (five rabbits

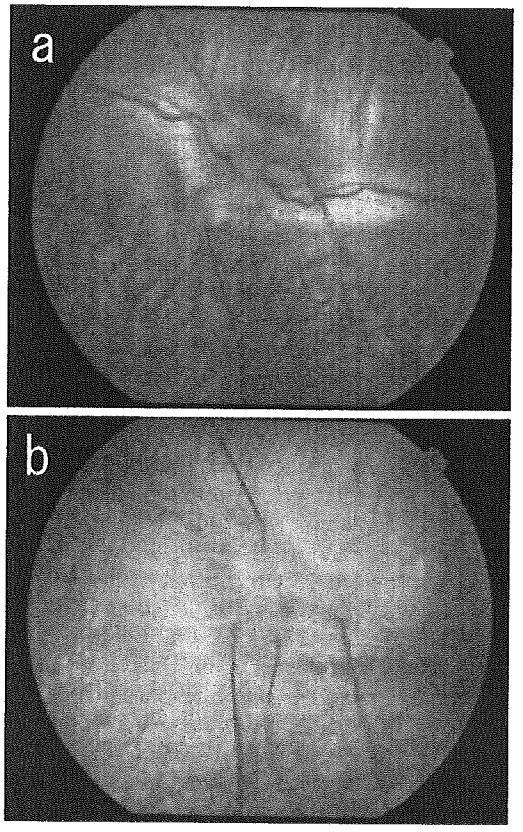

Fig. 1 **a** Fundus photograph and **b** fluorescein angiogram of a rabbit eye with four electrodes implanted 6 months earlier. The electrodes are stable without serious complications, and no abnormal fluorescein leakage is observed on the optic nerve head

each time before and at 1, 2, 3, and 4 months after implantation; three rabbits each time at 5 and 6 months after implantation). The mean relative implicit time and amplitude of a- and b-wave of ERGs (implanted/control) prior to implantation and at 1, 2, 3, 4, 5, and 6 months after implantation are shown in Table 1. The differences in mean relative implicit times and amplitudes of a- and b-waves between the implanted eyes and untreated control eyes were not statistically significant at any recording point throughout the post-implantation period ($P>0.05$ for all; Fig. 2).

Visually evoked potentials

VEPs were recorded before implantation and at 1-month intervals after implantation. The VEPs were elicited by stimulating the implanted and untreated control eyes of each of the rabbits separately (five rabbits each time before and at 1, 2, 3, and 4 months after implantation; three rabbits each time at 5 and 6 months after implantation). The mean implicit time of the P1 component of the implanted eyes was 23.6±1.4 ms (mean±standard deviation) before implantation and did not change significantly after implantation. The mean relative implicit times and amplitudes of the P1 component of VEPs (implanted/control) on the day of implantation and at 1, 2, 3, 4, 5, and 6 months after implantation are shown in Table 1. The differences in the relative implicit times and amplitudes of the P1 component of VEPs between the implanted eyes and untreated control eyes were not statistically significant at any recording point throughout the post-implantation period ($P>0.05$ for all; Fig. 3).

Electrically evoked potentials

Electrically evoked cortical potentials were elicited by bipolar electrical stimulation of the optic nerve using different combinations of the four electrodes in all of the eyes on the day of implantation and at 1-month intervals after implantation, except for one dislocated electrode (five eyes each time on the operation day and at 1, 2, 3, and 4 months after operation; three eyes each time at 5 and 6 months after operation). EEPs could be elicited by each combination of electrodes and the waveforms of EEPs did not differ significantly throughout the postimplantation period.

The mean implicit time of EEPs was 8.2±0.6 ms on the day of implantation, and it did not change significantly after implantation (data not shown). The amplitude of EEPs increased with increasing stimulus currents, and the current thresholds for the different electrode pairs in all of the implanted eyes were in the range 5–30 μA immediately after implantation on the operation day and 30–150 μA, 50–200 μA, 50–250 μA, 50–200 μA, 100–200 μA, and 75–200 μA at 1, 2, 3, 4, 5, and 6 months after implantation, respectively. The mean current threshold (charge densities) for eliciting EEPs was 19.3±9.2 μA (6.0± 2.9 $\mu C/cm^2$) immediately after implantation. The mean current threshold increased significantly to 78.8±31.9 μA (24.6±10.0 $\mu C/cm^2$) at 1 month after implantation and did not change significantly thereafter (Table 1 and Fig. 4).

Scanning electron microscopy

A thin layer of vitreous film was observed over the surface of the intravitreal segment of the electrodes that were

Table 1 Summary of ERG, VEP, and EEP results. The mean threshold currents (charge densities) to evoke EEPs increased significantly at 1 month after implantation, but did not change significantly thereafter. The implicit time and amplitude of the a- and b-waves of the ERGs and of P1 of the VEPs did not change significantly throughout the post-implantation period

Time	*n*	ERGs				VEPs		EEPs
		a-wave		b-wave		P1		
		Implicit time	Amplitude	Implicit time	Amplitude	Implicit time	Amplitude	Threshold μA(μC/cm²)
		(experimental/control eye, mean±standard deviation, %)						
Before or on day of implantation	5	97.5±6.8	92.3±7.9	89.8±11.6	86.3±14.4	97.7±9.8	100.7±14.5	19.3±9.2 (6.0±2.9)
After implantation								
One month	5	91.8±2.9	96.0±17.9	102.8±14.7	83.5±19.6	105.1±7.4	101.5±15.2	78.8±31.9 (24.6±10.0)
Two months	5	100.1±3.3	92.3±23.6	91.5±9.1	88.1±14.6	108.4±19.1	112.2±16.5	116.5±58.0 (36.4±18.1)
Three months	5	100.8±4.5	107.0±10.5	99.8±4.0	106.1±8.4	103.2±5.4	98.2±17.4	139.7±50.4 (43.7±15.8)
Four months	5	94.8±3.5	94.5±21.1	97.1±4.6	90.5±8.1	107.7±14.5	115.2±49.7	131.1±45.1 (41.0±14.1)
Five months	3	101.6±2.3	104.5±13.6	101.2±3.5	106.2±16.5	101.3±4.6	116.7±39.5	156.7±40.4 (49.0±12.6)
Six months	3	99.0±4.7	105.7±8.1	102.3±4.4	104.6±6.7	102.2±7.6	112.6±26.1	144.3±29.2 (45.1±9.1)

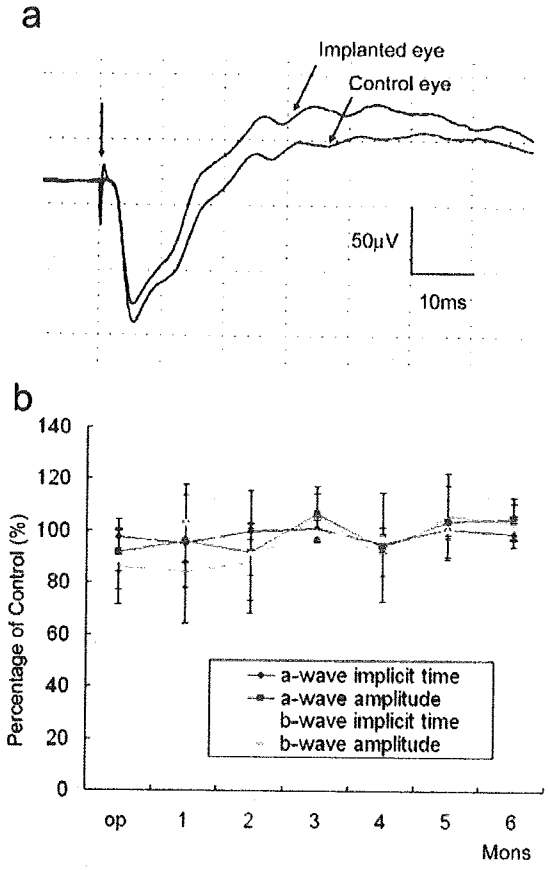

Fig. 2 **a** ERGs recorded from the implanted eye and untreated control eye at 6 months after implantation. **b** The mean amplitude and implicit time of the a- and b-waves for the eyes over the experiment period. The mean amplitudes and implicit times did not change significantly. The data at 5 and 6 months after implantation were calculated from the three remaining eyes. The values are expressed as percentages of those in the control eye of the same rabbit. Values are given as means±standard deviations. *op*, Operation day; *Mons*, months

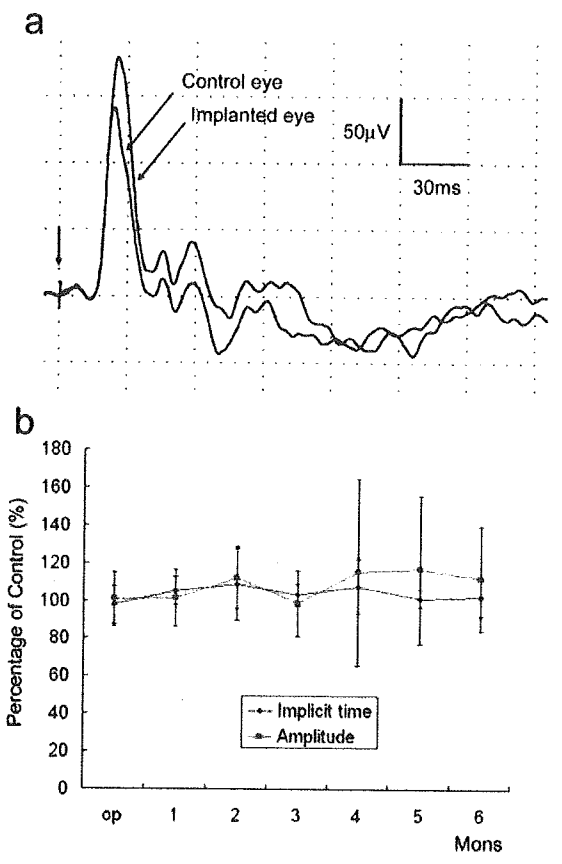

Fig. 3 **a** VEPs elicited from stimulating the implanted eye and untreated control eye at 6 months after implantation. **b** Mean amplitude and implicit time of P1 of the VEPs in the eyes over the experimental period. The mean amplitude and implicit time of P1 did not change significantly. The data at 5 and 6 months after implantation were analyzed for the three remaining eyes. The values are expressed as percentages of those in the control eye of the same rabbit. Values are given as means±standard deviations. *op*, Operation day; *Mons*, months

examined directly after removal from the implanted eyes. No structural degradation was observed on the surface of the intravitreal part of electrodes that were examined after cleaning (Fig. 5).

Histological study

None of the electrode tips were observed extruding outside the retrobulbar segment of the optic nerve close to the disc macroscopically in any of the five enucleated eyes. This indicated that the electrode tips were positioned and maintained within the optic nerve. Histological examination of longitudinal sections of the optic nerve heads revealed the positions of the intrapapillary electrodes in all implanted eyes. Not all of the electrodes were implanted parallel to the optic nerve fibers; most were obliquely positioned inside the optic nerve fiber. Photomicrographs of a histological section of the optic nerve head from two eyes at 6 months after implantation are shown in Fig. 6. The electrodes inside the optic disc are surrounded by a sheath of connective tissue of different thicknesses; some were enclosed by a very thin compact sheath of connective tissue and others had a thicker sheath. Mild infiltration of inflammatory cells was observed near the electrodes in some of the implant sites. The ganglion cell axons and interstitial cells near the electrodes appeared to be normal in the five eyes.

GFAP immunopositivity was detected in all astrocytes within the optic nerve and in the inner retina of untreated

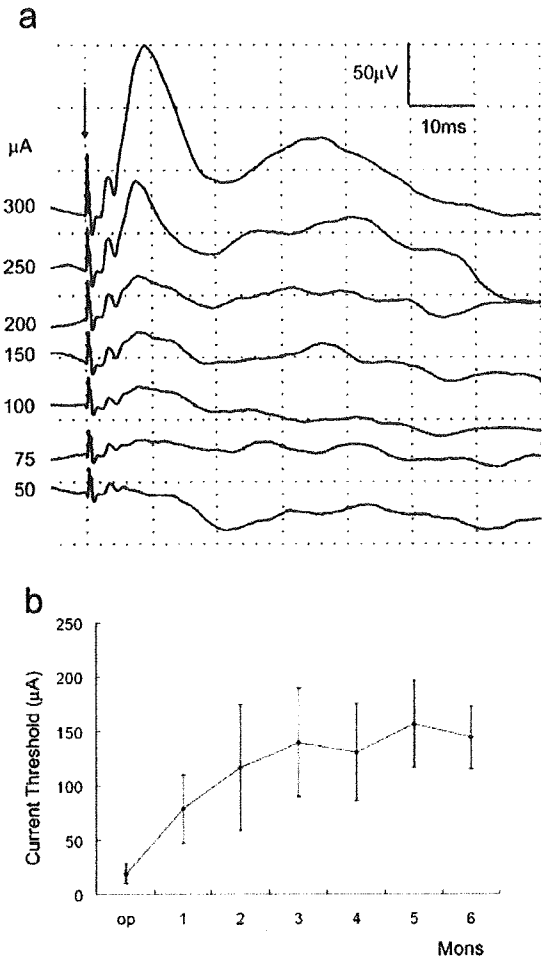

Fig. 4 **a** EEP waveforms elicited by bipolar electrical stimulating of the implanted eye using one pair of the four electrodes with different current intensities at 6 months after implantation. Note that the major positive EEP component peak at approximately 8 ms represents the cortical response. The major positive peak of EEPs was just detectable when the current was 75 μA, which was assessed as the current threshold in this examination session. **b** Mean stimulation current threshold for eliciting EEPs over the experimental period. The mean stimulation current threshold had increased significantly by 1 month after implantation and did not change significantly thereafter. The data at 5 and 6 months after implantation were obtained from the three remaining rabbits. Values are given as means±standard deviations. *op*, operation day; *Mons*, months

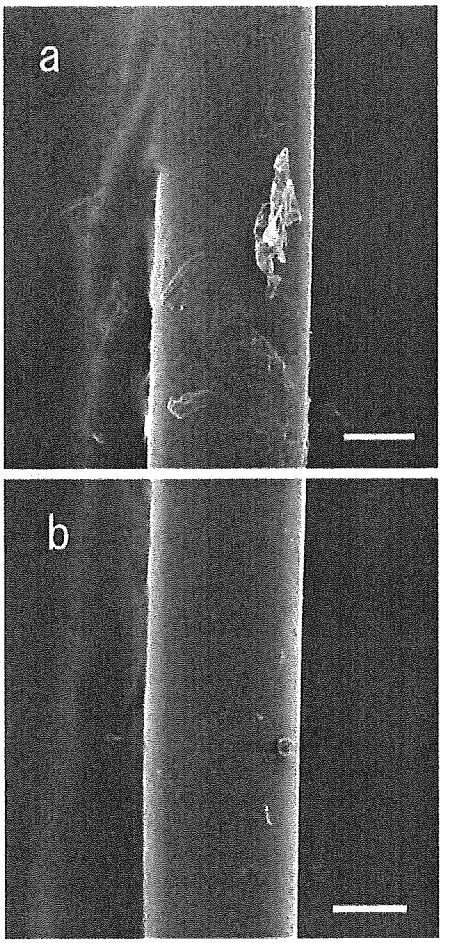

Fig. 5 Scanning electron microphotographs of the wire electrodes from a rabbit eye at 6 months after implantation. **a** The surface of the intraocular segment of the wire was covered with a thin layer of vitreous. **b** The surface of the intraocular part of the wire electrode appeared intact. The surface of the electrode was cleaned prior to processing in (**b**). (*Scale bars* 30 μm)

control eyes (Fig. 7a). The expression of GFAP increased under the surface of the optic nerve head of the implanted eyes (Fig. 7b,c; arrows). No GFAP staining was observed in the connective tissue encapsulations around the electrodes. No labeling was found in negative control preparations (Fig. 7d).

Discussion

The purpose of our experiment was to determine whether transscleral intrapapillary multiple wire microelectrodes can be used as stimulating electrodes of an optic nerve-based prosthesis. Previous studies conducted in our laboratory had demonstrated that the acute implantation of the transscleral wire microelectrodes into the optic nerve head is surgically and functionally feasible with minimal damage to the optic nerve in rabbit eyes [10, 27]. Our present results showed that 19 of the 20 transscleral intrapapillary wire microelectrodes were well stabilized and tolerated in the eyes over the 4–6 month follow-up period without se-

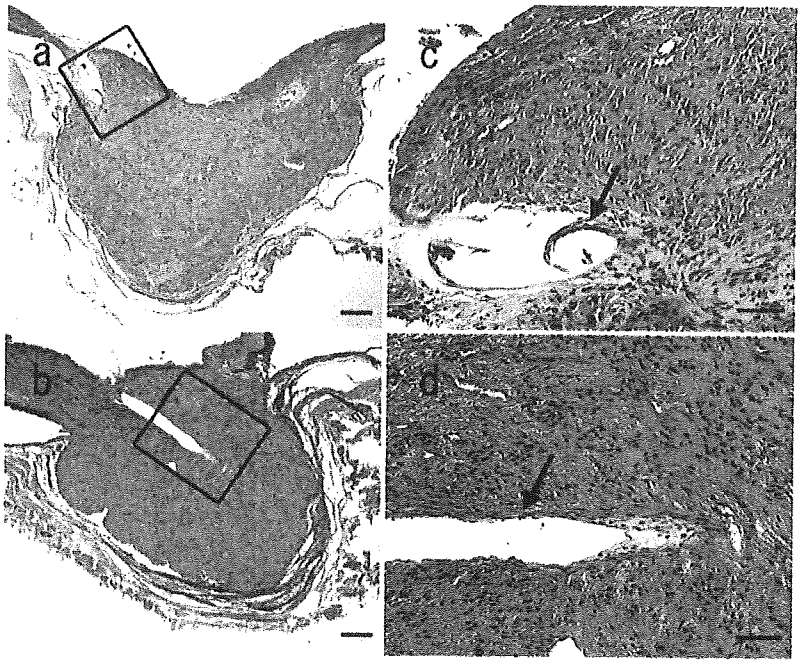

Fig. 6 Light photomicrographs of longitudinal sections of optic nerve heads from two different eyes at 6 months after implantation. **a** A section of an optic nerve head through one site of electrode from one implanted eye. **b** A section of an optic nerve head through one site of electrode from another implanted eye. **c** High magnification of the square in (**a**). Mild infiltration of inflammatory cells and a thin connective tissue encapsulation are observed around the electrode site (*arrow*). Ganglion cell axons near the electrode trunk appeared to be normal. **d** High magnification of the square in (**b**). A very thin connective tissue encapsulation is observed around the electrode site (*arrow*). (Hematoxylin–eosin staining; *scale bars*: **a**, **b** 200 μm, **c**, **d** 50 μm)

rious complications. The tissue reaction associated with the implanted electrodes was mild and confined to the insertion sites. More importantly, the visual cortex could be activated by direct electrical stimulation of the optic nerve axons with approximately the same current charge from 1 month after implantation. Our data demonstrated that the chronic implantation of transscleral intrapapillary microelectrodes appears to be safe and effective.

We are aware that the spatial resolution by an optic nerve-based prosthesis is limited in comparison with epi-

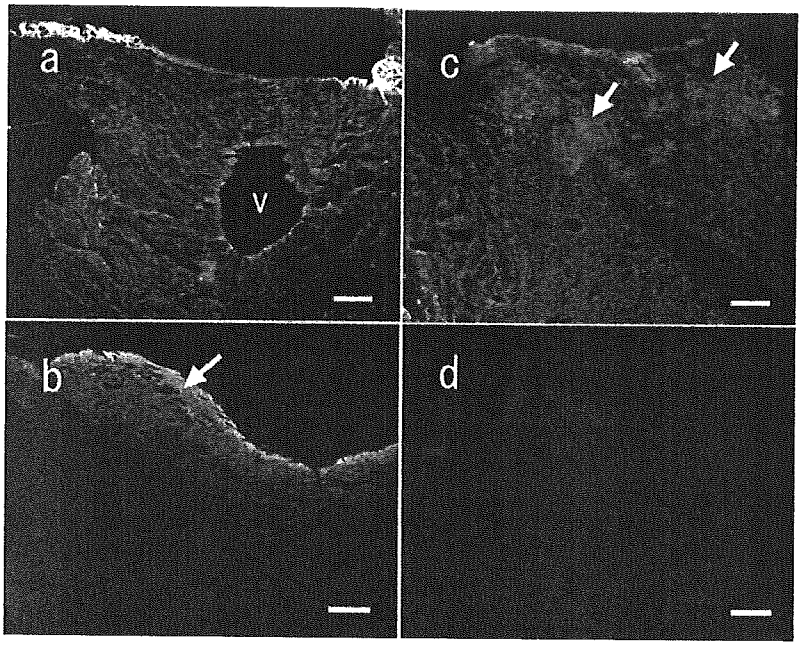

Fig. 7 Fluorescence photomicrographs of immunohistochemical staining of longitudinal sections of optic nerve heads using antibodies against GFAP. **a** A section of an optic nerve head from an untreated control eye. All astrocytes in the optic nerve head are intensely stained vessel. **b** Section of an optic nerve head through one site of electrodes from the eye shown in Fig. 6a. **c** Section of an optic nerve head through one site of electrodes from the eye shown in Fig. 6b. An increase of staining is observed under the surface of the optic nerve head and no GFAP staining is observed within the encapsulations around electrodes in the implanted eyes shown in Fig. 6 (*arrows*). **d** No labeling can be seen in the negative control section (*Scale bars* 100 μm)

retinal and subretinal prostheses, because the electrical pulses of a small area of a highly packed concentration of axons will activate axons representing a wide area of the visual field. However, a cuff electrode will activate neurons over a much larger area, and thus good selective stimulation is theoretically more difficult to achieve with a cuff electrode than with penetrating microelectrodes.

The significant advantages of microstimulation with a penetrating electrode in the central nervous system and peripheral nerves have been extensively investigated for developing a neuroprosthesis [3–5, 15, 25]. Bak et al. have shown the possibility of highly specific microstimulation of the retino-thalamocortical projection in the visual cortex [3]. Multi-microelectrode arrays have been shown to achieve high spatio-temporal resolution of the visual pathways [22]. A highly selective stimulation has been obtained with a penetrating microelectrode array placed within the fascicles of cat sciatic nerve that can activate different muscle groups with low stimulation currents in acute and long-term experiments [4, 5]. A successful electrically evoked auditory brainstem response has been recorded with penetrating electrodes with lower thresholds than surface electrodes [25]. Because pattern recognition has been somewhat successful with optic nerve stimulation using a cuff electrode placed around the optic nerve [34], it is reasonable to expect that more selective and localized microstimulation of axons by an intrapapillary microelectrode array with low charge density would activate functionally distinct subunits within the optic nerve and provide blind patients with relatively better visual resolution.

We inserted four wire electrode tips directly into the edges of the optic disc and carefully fixed the extraocular parts of the electrodes to the sclera. The first suture at the entrance was crucial in preventing the electrode tips from dislodging from their original implanted position. Considering the absence of complex vitreoretinal procedures, the very small dimension of electrodes, and relatively good biocompatibility of the electrode material used, we did not perform vitrectomy prior to electrode insertion because our nonvitrectomizing vitreous surgery in eyes for idiopathic epimacular proliferation had demonstrated that retinal tears and proliferative reactions did not occur after nonvitrectomizing simple vitroretinal manipulation surgery [29]. Throughout the post-implantation period, almost all of the transscleral wire electrodes were quiet and well tolerated with their tips in the original implanted positions. Thus, our results encouraged us to identify the consequences of long-term intrapapillary wire microelectrode implantation. No infection was found in the cul-de-sac and intraocular cavity, and no vitreoretinal proliferation reaction and fibrous encapsulation of the electrodes were observed on ophthalmologic examination of any of the five eyes.

Our observations were consistent with previously reported findings that prolonged transscleral epiretinal implants were well tolerated without ocular infection as long as they were positioned subconjunctivally and the scleral wound was tightly sealed [16]. The slightly distorted appearance of the optic nerve head observed in one eye may have been due to the mild movement of the electrodes on the optic nerve head associated with eye movements.

The development of radial optic neurotomy for the treatment of central retinal venous occlusion demonstrated that surgical manipulation of the optic disc is potentially possible [23] and prompted us to select the optic nerve head as the electrode implantation site for reasons of anatomy and surgical accessibility. However, a focal vision field defect related to the site of neurotomy was detected in some patients, indicating damage to optic nerve fibers or the blood supply of the optic nerve head following surgical manipulation on the optic nerve head [37]. The platinum wire electrodes used were much thinner (50 μm diameter) than the microvitreoretinal knife used in the radial optic neurotomy surgery. Our results showed that the tissue damage and response to the intrapapillary electrode implantation were mild and limited to the vicinity of the insertion site.

Previous studies on the histological changes following long-term microelectrode implantation in cat sciatic nerve and cochlear nucleus reported that the morphology of the nerve around the electrodes and tips was normal except for glial sheathing, even after continuous microstimulation [5, 20]. The tissue responses found in our eyes are believed to be the result of the presence of the electrodes because we did not perform long-term continuous electrical stimulation of the optic nerve. Histological evaluations of our eyes confirmed that the neuronal tissues near the insertion sites were well preserved. The increased expression of GFAP in the optic nerve after electrode implantation is in agreement with the reported findings that GFAP expression readily increases under stress conditions and intraocular manipulations [9, 32]. Hypertrophy of glial cells and connective tissue structures within the optic nerve head have often been observed in patients in the end stage of retinitis pigmentosa.

The histological changes found in this study were also in agreement with our electrophysiological findings. The VEPs did not change significantly, and EEPs could be elicited by electrical stimulation with any pair of electrodes at each follow-up examination over the post-implantation period. This indicated that the majority of the ganglion cell axons functioned well.

The average implicit time of the EEPs (8.2±0.6 ms) was approximately one-third of that for the VEPs (23.6±1.4 ms). This difference must be due to the time required for the activation of the photoreceptors and for the signals to reach the ganglion cells. The mean current threshold (charge density) for detecting EEPs was 19.3±9.2 μA (6.0±2.9 $\mu C/cm^2$) immediately after implantation, which was very similar to our previous acute results [10]. Charge

thresholds for eliciting cortical response in animal experiments vary because of differences in the electrical properties of the stimulation electrode, the size and geometry of the electrodes, the type of recording electrode, and the stimulation parameters. Cortical responses have been reported to be elicited by average charge densities of 2.8 nC/cm^2 [7] and 50 μC/cm^2 [11] with acute subretinal electrical stimulation in rabbits. The large size of the stimulation device used by Chow et al. most likely explains their extremely low charge density [7]. Theoretically, it should be easier to activate the cortical response by direct optic nerve stimulation than by subretinal stimulation. Our study demonstrated that cortical response could be activated by direct optic nerve with low charge thresholds. The mean threshold current in our study was similar to that with epiretinal electrode stimulation in rabbits. Water et al. reported that the threshold for eliciting EEPs was 1–12 μC/cm^2 in a rabbit model [36]. The possibility of activating ganglion cell axons should exist, although the ganglion cell body is more likely to be activated by epiretinal electrical stimulation.

The mean stimulation threshold for eliciting EEPs increased to 78.8±31.9 μA (24.6±10.0 μC/cm^2) at 1 month after implantation, but remained approximately constant thereafter. The change of stimulation threshold was most likely due to the limited tissue response to the presence of the electrodes, because the encapsulation process is most active in the first several weeks after implantation [5]. The resistance of the encapsulating tissue has also been shown to alter the shape and magnitude of the electric field generated by chronically implanted electrodes [12]. The growth of the encapsulation at the interface between the electrode and the optic nerve fiber may, to some extent, generate a barrier for electrical signal conduction or cause a greater spread of the current by short-circuiting, in which case higher current densities would be needed for successful electrical stimulation. Our results are consistent with another reported finding that the median stimulation threshold increased by a factor of 3.5 within the first month and changed little thereafter in experimental long-term stimulation and recording with a penetrating microelectrode array in the cat sciatic nerve [5].

Although we cannot decisively estimate the influence of long-term continuous electrical stimulation on the optic nerve fiber from our results, the extent of tissue encapsulation around the electrodes has been shown to be similar to that around stimulated electrodes as long as the stimulation is at a safe, non-damaging level [1].

The positive effect of electrical stimulation on the nerve fiber has also been extensively studied. Electrical stimulation has been demonstrated to promote sprouting and some early functional recovery [17]. Short- and long-term continuous electrical stimulation was reported to accelerate the regeneration of transected motor axons and preferential motor reinnervation [2]. Recently, Morimoto et al. [21] showed that in vivo electrical stimulation on the optic nerve with currents weaker than 70 μA for 2 h could enhance the survival of ganglion cells. Weak electrical stimulation by a current of 0.1 mA for 0.1 s has been shown to increase the blood circulation of the optic nerve head [31]. The threshold stimulation current for axonal injury has been shown to be greater than the current required to excite all of the nerve axons [19]. We suggest that as long as the electrical stimulation to the optic nerve is within safe limits, it would be unlikely to induce neural damage, although the margin of safety has not yet been determined and the possibility of damage due to continuous electrical stimulation is not definitely excluded.

The wire electrodes used in our experiment are made of platinum wire coated with epoxy resin. Platinum is a proven biocompatible electrode material and is widely used for long-term neural stimulating electrodes because of its superior charge transfer properties [6]. However, the effect of epoxy resin on the retina has not yet been examined. No changes were observed on the surface of the electrodes even up to 6 months after implantation by funduscopic examination. SEM also revealed the structural integrity of the wire electrodes, and no post-implantation mechanical degradation or corrosion of wire electrodes was detected. Moreover, ERGs and VEPs did not change significantly, indicating that the function of the retina remained normal over the post-implantation period. However, a longer time effect of epoxy resin on the retina needs to be examined for permanently implanted intraocular electrodes. The investigation could reveal an electrode coated with a proven biocompatible material would be a better alternative.

In conclusion, our data demonstrate that long-term transscleral intrapapillary wire microelectrode implantation appears to be safe and effective and should be considered for future optic nerve-based prostheses. Many issues remain to be investigated, e.g., field responses and their topological correspondences and spatial extent to the selective stimulation of optic nerve fibers by such an intrapapillary multimicroelectrode array, the margins of safety of electrical stimulation, and the character and design of the electrodes. In addition, surgical technique may need to be improved for long-term implantation. For prolonged implantation, it seems reasonable to perform vitrectomy and intraocular fixation of the electrodes to prevent them pulling out of the implant position. We are investigating these important issues in ongoing experiments.

Acknowledgements This study was supported by a grant (no. 14571670) from the Ministry of Education, Culture, Sports, Science and Technology, Japan.

References

1. Agnew WF, McCreery DB, Yuen TG, Bullara LA (1989) Histologic and physiologic evaluation of electrically stimulated peripheral nerve: considerations for the selection of parameters. Ann Biomed Eng 17:39–60
2. Al-Majed AA, Neumann CM, Brushart TM, Gorgon T (2000) Brief electrical stimulation promotes the speed and accuracy of motor axonal regeneration. J Neurosci 20:2602–2608
3. Bak M, Girvin P, Hambrecht FT, Kufta CV, Loeb GE, Schmidt EM (1990) Visual sensations produced by intracortical microstimulation of the human occipital cortex. Med Biol Eng Comput 28:257–259
4. Branner A, Stein RB, Normann RA (2001) Selective stimulation of cat sciatic nerve using an array of varying-part microelectrodes. J Neurophysiol 85:1585–1594
5. Branner A, Stein RB, Fernandez E, Aoyaki Y, Normann RA (2004) Long-term stimulation and recording with a penetrating microelectrode array in cat sciatic nerve. IEEE Trans Biomed Eng 51:146–157
6. Brummer SB, Turner MJ (1977) Electrochemical considerations for safe electrical stimulation of the nerve system with platinum electrodes. IEEE Trans Biomed Eng 24:59–63
7. Chow AY, Chow VY (1997) Subretinal electrical stimulation of the rabbit retina. Neurosci Lett 225:13–16
8. Delbeke J, Wanet-Defalque MC, Gerard B, Troosters M, Michaux G, Veraat C (2002) The microsystems based visual prosthesis for optic nerve stimulation. Artif Organs 26:232–234
9. Fang XY, Hayashi A, Morimoto T, Usui S, Cekic O, Fujioka, Hayashi N, Fujikado T, Ohji M, Tano Y (2004) Retinal changes after macular translocation with 360-degree retinotomy in monkey eyes. Am J Ophthalmol 137:1034–1041
10. Fang XY, Sakaguchi H, Fujikado T, Osanai M, Kanda H, Ikuno Y, Kamei M, Ohji M, Gan DK, Choi J, Yagi T, Tano Y (2005) Direct stimulation of optic nerve by electrodes implanted in optic disc of rabbit eyes. Graefes Arch Clin Exp Ophthalmol 243:49–56
11. Gekeler F, Kobuch K, Schwahn HN, Stett A, Shinoda K, Zrenner E (2004) Subretinal electrical stimulation of the rabbit retina with acutely implanted electrode arrays. Graefes Arch Clin Exp Ophthalmol 242:587–596
12. Grill WM, Mortimer JT (1994) Electrical properties of implant encapsulation tissue. Ann Biomed Eng 22:23–33
13. Humayun MS, de Juan E Jr, Weiland JD, Dagnelie G, Katona S, Greenberg R, Suzuki S (1999) Pattern electrical stimulation of the human retina. Vision Res 39:2569–2576
14. Kanda H, Morimoto T, Fujikado T, Tano Y, Fukuda Y, Sawai H (2004) Electrophysiological studies of the feasibility of suprachoroidal-transretinal stimulation for artificial vision in normal and RCS rats. Invest Ophthalmol Vis Sci 45:560–566
15. Liu X, McPhee G, Seldon HL, Clark GM (1997) Histological and physiological effects of the central auditory prosthesis: surface versus penetrating electrodes. Hearing Res 114:264–274
16. Majji AB, Humayun MS, Weiland JD, Suzuki S, D'anna SA, de Juan E Jr (1999) Long-term histological and electrophysiological results of an inactive epiretinal electrode array implantation in dogs. Invest Ophthalmol Vis Sci 40:2073–2081
17. Manivannan S, Terakawa S (1994) Rapid sprouting of filopodia in nerve terminals of chromaffin cells, and dorsal root neurons induced by electrical stimulation. J Neurosci 14:5917–5928
18. Margalit E, Maia M, Weiland JD, Greenberg RJ, Fujii GY, Torres G, Piyathaisere DV, O'Hearn TM, Liu W, Lazzi G, Dagnelie G, Scribner DA, de Juan E Jr, Humayun MS (2002) Retinal prosthesis for the blind. Surv Ophthalmol 47:335–356
19. McCreery DB, Agnem WF, Yuen TG, Bullara LA (1992) Damage in peripheral nerve from continuous electrical stimulation: comparison of two stimulus waveforms. Med Biol Eng Comput 30:109–114
20. McCreery DB, Yuen TG, Agnem WF, Bullara LA (1997) A characterization of the effects on neuronal excitability due to prolonged microstimulation with chronically implanted microelectrodes. IEEE Trans Biomed Eng 44:931–939
21. Morimoto T, Miyashi T, Fujikado T, Tano Y, Fukuda Y (2002) Electrical stimulation enhances the survival of axotomized retinal ganglion cells in vivo. Neuroreport 13:227–229
22. Normann RA, Warren DJ, Ammermuller J, Fernandez E, Guillory S (2001) High-resolution spatio-temporal mapping of visual pathways using multi-electrode arrays. Vis Res 41:1261–1275
23. Opremack EM, Bruce RA, Lomeo MD, Ridenour CD, Letson AD, Rehmar AJ (2001) Radial optic neurotomy for central retinal vein occlusion: a retrospective pilot study of 11 consecutive cases. Retina 21:408–415
24. Rizzo JF III, Wyatt J, Humayun M, de Juan E, Liu W, Chow A, Eckmiller R, Zrenner E, Yagi T, Abrams G (2001) Retinal prosthesis: an encouraging first decade with major challenges ahead. Ophthalmology 108:13–14
25. Rosahi SK, Mark G, Herzog M, Pantazis C, Ghaarabaghi F, Matthies C, Brinker T, Samii M (2001) Far-field responses to stimulation of the cochlear nucleus by microsurgically placed penetrating and surface electrodes in the cat. J Neurosurg 95:845–852
26. Sakaguchi H, Fujikado T, Fang XY, Kanda H, Osanai M, Nakauchi K, Ikuno Y, Kamei M, Yagi T, Nishimura S, Ohji M, Yagi T, Tano Y (2004) Transretinal electrical stimulation with a suprachoroidal multichannel electrode in rabbit eyes. Jpn J Ophthalmol 48:256–261
27. Sakaguchi H, Fujikado T, Kanda H, Osanai M, Fang XY, Nakauchi K, Ikuno Y, Kamei M, Ohji M, Yagi T, Tano Y (2004) Electrical stimulation with a needle type electrode placed into the optic nerve in rabbit eyes. Jpn J Ophthalmol 48:552–557
28. Santos A, Humayun MS, de Juan E Jr, Greenberg BJ, Marsh MJ, Klock IB, Milam AH (1997) Preservation of the inner retina in retinitis pigmentosa. Arch Ophthalmol 115:511–515
29. Sawa M, Saito Y, Hayashi A, Kusaka S, Ohji M, Tano Y (2001) Assessment of nuclear sclerosis after nonvitrectomizing vitreous surgery. Am J Ophthalmol 132:356–362
30. Schwahn HN, Gekeler F, Kohler K, Kobuch K, Sachs HG, Schulmeyer F, Jakob W, Gabel VP, Zrenner E (2001) Studies on the feasibility of a subretinal visual prosthesis: data from Yucatan micropig and rabbit. Graefes Arch Clin Exp Ophthalmol 239:961–967

31. Sugiyama T, Hara H, Oku H, Nakatsuji S, Okuno T, Sasaoka M, Ota T, Ikeda T (2001) Optic cup enlargement followed by reduced optic nerve head circulation after optic nerve stimulation. Invest Ophthalmol Vis Sci 42:2843–2848
32. Varela HJ, Hernandez MR (1997) Astrocyte responses in human optic nerve head with primary open-angle glaucoma. J Glaucoma 6:303–313
33. Veraart C, Raftopoulos C, Mortimer JT, Delbeke J, Pins D, Michaux G, Vanlierde A, Parrini S, Wanet-Defalque MC (1998) Visual sensations produced by optic nerve stimulation using an implanted self-sizing spiral cuff electrode. Brain Res 813:181–186
34. Veraart C, Wanet-Defalque MC, Gérard B, Vanlierde A, Delbeke J (2003) Pattern recognition with the optic nerve visual prosthesis. Artif Organs 27:996–1004
35. Walter P, Szurman P, Vobig M, Berk H, Ludtke-Handjery HC, Richter H, Mittermayer C, Heimann K, Sellhaus B (1999) Successful long-term implantation of electrically inactive epiretinal microelectrode arrays in rabbits. Retina 19:546–552
36. Water P, Heimann K (2000) Evoked cortical potentials after electrical stimulation of the inner retina in rabbits. Graefes Arch Clin Exp Ophthalmol 238:315–318
37. Williamson TH, Poon W, Whitefield L, Strothidis N, Javcock P, Strothoudis N (2003) A pilot study of pars plana vitrectomy, intraocular gas, and radial neurotomy in ischaemic central retinal vein occlusion. Br J Ophthalmol 87:1126–1129

Ophthal. Physiol. Opt. 2006 **26:** 65–70

Wavefront analysis of eyes with cataracts in patients with monocular triplopia[1]

Aya Kim[1], Kenichiro Bessho[2], Yoshitaka Okawa[2], Naoyuki Maeda[1], Yasuo Tano[1], Yoko Hirohara[3], Toshifumi Mihashi[3] and Takashi Fujikado[2]

[1]Department of Ophthalmology, Osaka University Graduate School of Medicine, Osaka, [2]Department of Applied Visual Science, Osaka University Graduate School of Medicine, Osaka, and [3]Technical Research Institute, Topcon Corporation, Tokyo, Japan

Abstract

Purpose: To determine whether wavefront analysis using a Hartmann–Shack (H-S) aberrometer can reveal the cause of monocular triplopia in eyes with mild cataracts.

Methods: Six patients (nine eyes; age range 38–58 years; average 49.8 ± 6.9 years) who complained of monocular triplopia at the Osaka University Hospital between January and December 2003 were examined. Wavefront analyses of ocular and corneal aberrations of the central 4 mm diameter were performed using a H-S aberrometer equipped with a Placido ring videokeratoscope. The ocular and corneal higher-order wavefronts were fitted with a fourth-order Zernike expansion.

Results: All nine eyes showed mild nuclear cataract and had a mean spherical refractive error of −10.3 ± 3.5 D. The visual acuity was ≥ 20/40 except in one eye with glaucoma. For the Zernike polynomials, the trefoil aberration (C3-3) and the spherical aberration (C40) were significantly higher than those of age-matched normal controls ($p < 0.001$). The simulated retinal image of a Landolt C showed that the combination of trefoil aberration and the spherical aberration can cause an image with a triple configuration.

Conclusions: Monocular triplopia was reported by middle-aged patients with mild nuclear cataract and high myopia. Wavefront analyses suggested that the triple configuration was caused by the combined increase of the trefoil and spherical aberration in lenses with mild nuclear cataracts.

Keywords: monocular diplopia, nuclear cataract, spherical aberration, trefoil aberration, triplopia, wavefront analysis

Introduction

Monocular polyopia has been reported by patients with different types of ocular conditions or diseases. Refractive error (Coffeen and Guyton, 1988; Woods *et al.*, 1996a), near work (Bowman *et al.*, 1978; Goss and Criswell, 1992a; Mandell, 1996; Ford *et al.*, 1997; Golnik and Eggenberger, 2001), corneal distortions (Carney *et al.*, 1981; Kommerell, 1993; Campbell, 1998), and lens abnormalities such as cataracts or subluxated lenses (Fincham, 1963; Woods *et al.*, 1996b) can cause monocular polyopia. Monocular polyopia has also been reported following refractive surgery, and even retinal abnormalities, such as an epiretinal membrane, and cerebral lesions can cause monocular polyopia (Trobe, 2001; Lee and Brazis, 2003).

The most common clinical examination to determine if the monocular polyopia is caused by optical aberrations in the eye is the pinhole test. Monocular triplopia has been reported by middle-aged patients with mild nuclear cataract (Kluxen, 1985; Kaufman and Sugar, 1996) and we have reported the wavefront analysis of one such case of monocular triplopia in an eye with mild nuclear cataract (Fujikado *et al.*, 2004). Our analysis

Received: 7 March 2005
Revised form: 25 July 2005
Accepted: 7 August 2005

Correspondence and reprint requests to: Takashi Fujikado.
Tel.: +81 6 68793941; Fax: +81 6 68793948.
E-mail address: fujikado@ophthal.med.osaka-u.ac.jp

[1]Presented at ARVO meeting, Fort Lauderdale, FL, USA, April 27th 2004.

showed that the combination of trefoil aberration and spherical aberration was the most likely cause of the monocular triplopia in that patient. Although monocular polyopia is not that rare, the optical mechanisms of monocular triplopia are not well understood.

The purpose of this study was to examine nine eyes of six patients with cataracts who complained of monocular triplopia. They were examined with the H-S wavefront aberrometer, and the optical mechanism underlying the monocular triplopia was examined.

Methods

Patients

Six patients (nine eyes; age range 38–58 years; average 49.8 ± 6.9 years) who complained of monocular triplopia were examined at the Osaka University Hospital from January to December in 2003 (*Table 1*). The spherical equivalent of their subjective refraction ranged from −7.5 to −19.0 D with an average of −10.5 ± 4.0 D. The astigmatism ranged from 0 to 1.75 D with an average of 0.7 ± 0.8 D. The best-corrected visual acuity (BCVA) ranged from 20/40 to 20/15 (median, 20/25) except for one eye, which also suffered from glaucoma. A slit-lamp examination revealed a mild nuclear cataract in all eyes (*Figure 1*). Fundus examination showed glaucomatous changes of the optic disc in one eye, but otherwise no abnormal findings were observed in the other eyes (*Table 1*).

The control group included 18 eyes of 18 normal subjects who did not have ocular abnormalities except for mild refractive errors. The spherical equivalent of the refractive error measured by manifest refraction ranged from +1.75 to −6.0 D with an average −1.6 ± 2.3 D. Their ages ranged from 40 to 59 years with an average of 46.1 ± 5.6 years. The average age of control group was not statistically different from the triplopia group (Mann–Whitney Rank Sum Test).

Written informed consent was obtained from all patients and control subjects after an explanation of the potential risk of wavefront analysis was given. The procedures were performed to conform to the tenets of the Declaration of Helsinki.

Hartmann-Shack wavefront aberroscopy

The higher-order wavefront aberrations (third- to fourth-order wavefront Zernike aberrations) were obtained with a H-S wavefront analyzer (KR-9000PW, Topcon Co., Tokyo, Japan). Measurements were repeated at least three times for each eye to obtain a well focused, properly aligned image of the eye. The details of the H-S system have been described in detail elsewhere (Kuroda *et al.*, 2002a). Briefly, a superluminescent diode (SLD, $\lambda = 840$ nm) is attached to a single-mode optical fiber, and a lens system forms a point image on the retina. An aperture stop is placed in the lens system to limit the diameter of the light beam to 1 mm in the plane of the pupil for a single pass measurement. Light reflected from the point image on the retina is led to a H-S wavefront sensor through a lens system.

The H-S wavefront sensor consists of 169 small lenses aligned in a grid on a Hartmann plate and a cooled CCD. A number of point images are formed on the CCD, and the centroid of each point image is obtained to calculate the displacement of the point image from the reference point. The wavefront aberrations are calculated from the displacements and are expanded with the Zernike polynomials. The normalized values of Zernike polynomials were used for the statistical analysis. The co-ordinates were converted from vertex normal to pupillary center. The dynamic range of the wavefront sensor was set to ± 15 D and if the point images were able to be identified, the dynamic range was expanded by summing up the value of C 20.

Table 1. The baseline characteristics of patients

						Third-order aberration (μm)				Fourth-order aberration (μm)				
Case	Sex	Age	Eye	Spherical (D)	BCVA	C3-3	C3-1	C31	C33	C4-4	C4-2	C40	C42	C44
1	M	45	R	−9.75	20/20	−0.16	0.02	0.05	−0.01	0.05	−0.03	−0.19	−0.05	0.04
			L	−7.5	20/15	−0.16	−0.19	−0.04	0.01	0.00	−0.01	−0.18	0.00	0.03
2	F	58	R	−9.5	20/25	−0.11	−0.07	−0.12	0.01	−0.01	0.05	−0.13	−0.06	−0.03
			L	−8	20/25	−0.10	0.06	0.06	0.05	−0.07	−0.02	−0.15	−0.04	0.01
3	F	51	R	−13.5	20/25	−0.07	−0.03	−0.04	0.02	0.01	0.01	−0.14	−0.02	−0.03
4	F	45	R	−9	20/40	−0.18	0.04	−0.24	0.17	0.07	−0.07	−0.39	−0.06	−0.04
5	M	38	R[a]	−19	20/200	−0.24	−0.11	−0.08	0.11	0.08	0.08	−0.23	−0.18	−0.20
6	F	54	R	−8.5	20/20	−0.15	0.27	0.00	0.11	0.11	0.01	−0.31	−0.05	0.10
			L	−7.5	20/20	−0.11	−0.03	−0.02	0.00	−0.03	0.00	−0.27	0.01	0.03

M, male; F, female; R, right; L, left; Spherical, Spherical equivalent refractive error; D, diopter; BCVA, best corrected visual acuity.
[a]Denotes eye with glaucoma.

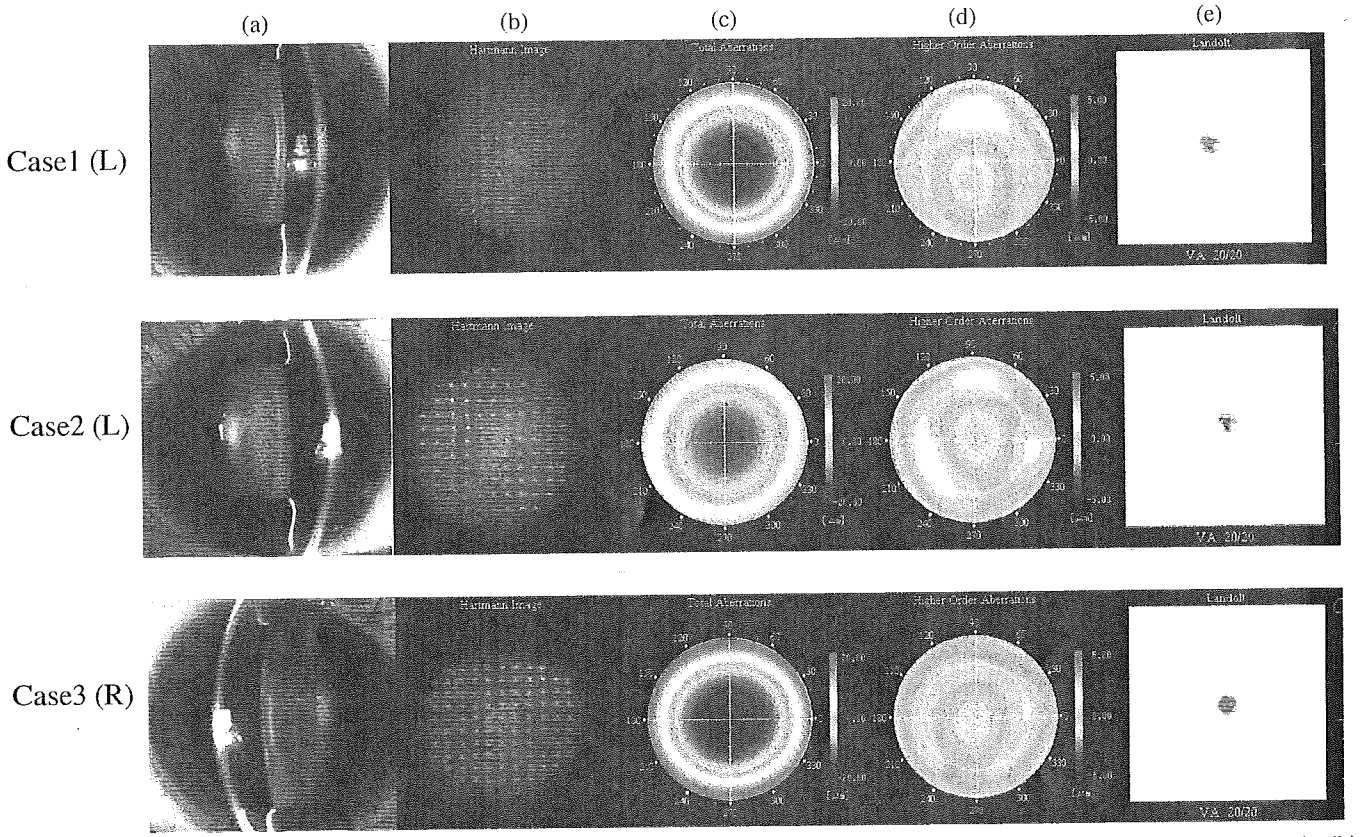

Figure 1. Slit-lamp photographs and results of wavefront analysis for cases 1–3. a. Slit-lamp photographs. All eyes (cases 1–3) showed mild nuclear cataract. b. H-S images. All eyes showed Concave-shaped H-S images. c. Color-coded maps of total aberration. All eyes showed high myopia. d. Color-coded maps of higher-order aberration. All eyes showed delayed wavefront in the center with cloverleaf-shaped advanced wavefront in the peripheral pupillary area. e. Simulated retinal images of Landolt C from higher-order aberrations. All eyes showed triple configuration of Landolt C.

For the simulation of retinal images, we used double Fast Fourier Transform (FFT) method to obtain the optical transfer function (OTF). This step consists of FFT of pupil function to obtain point spread function (PSF) and FFT of the PSF to obtain OTF. For pupil function, measured wavefront aberrations were used. Obtained OTF was multiplied by FFT of a Landolt C to obtain the simulated images.

The corneal topography was measured simultaneously using the Placido disk attached to the H-S wavefront analyzer, and the corneal aberration was calculated using the Zernike polynomials. The analysis of the aberrations was performed for a pupil dilated by an instillation of tropicamide and calculated for the central 4 mm diameter pupil. This was chosen to represent a typical pupil size under photopic conditions. The analyzed area for the corneal aberration was the same as for the ocular aberration.

Statistics

The comparisons of Zernike coefficients between the triplopia group and control group were performed by the *t*-test when the measurements were normally distributed and by the Mann–Whitney Rank Sum Test when they were not normally distributed.

Results

Among the coefficients of Zernike polynomials for the whole eye, the trefoil aberration (C3-3, −0.14 ± 0.06 μm) and the spherical aberration (C40, −0.21 ± 0.09 μm) were significantly higher than those of the age-matched controls (C3-3, −0.04 ± 0.05 μm, $p < 0.001$ and C40, 0.04 ± 0.01 μm, $p < 0.001$). Another trefoil aberration (C33, 0.05 ± 0.06 μm) and secondary astigmatism along 90° (C42, −0.05 ± 0.06 μm) were also significantly higher than in the controls (C33, −0.00 ± 0.05 μm, $p = 0.019$ and C42, 0.00 ± 0.02 μm, $p = 0.007$). The other third- and fourth-order Zernike coefficients in the triplopia group were not significantly different from those in the control group (*Figure 2*).

The corneal third- and fourth-order Zernike coefficients in the patients were not different from those of normal controls except for the vertical coma (C3-1,

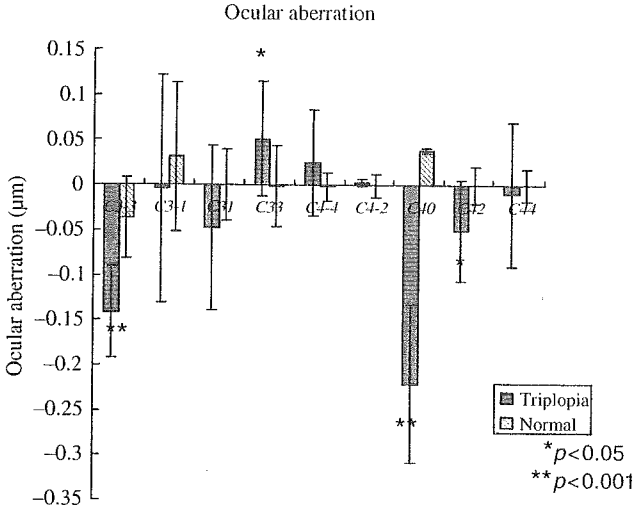

Figure 2. Comparison of Zernike terms for the whole eye between triplopia group and normal group. Trefoil aberration (C3-3) and spherical aberration (C40) were significantly larger in triplopia group than in normal control group ($p < 0.001$). The other trefoil aberration (C33) and one of the fourth-order aberrations (C42) were also larger in the triplopia group compared with normal group ($p < 0.05$).

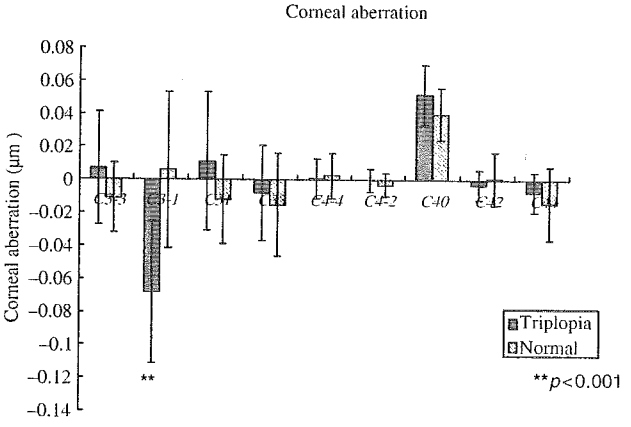

Figure 3. Comparison of corneal Zernike terms between triplopia group and normal group. Coma aberration (C3-1) was significantly larger in triplopia group compared with normal group ($p < 0.001$).

−0.07 ± 0.04 μm for triplopia group vs 0.01 ± 0.05 μm for normal controls, $p < 0.001$; *Figure 3*).

All eyes showed concave-shaped H-S images, high myopia, and delayed wavefront in the center with a cloverleaf-shaped advanced wavefront in the peripheral pupillary area (*Figure 1*). The simulated image of the Landolt C showed a triple configuration in all of the experimental eyes (*Figure 1*). The result of wavefront analysis concerning the right eye of case 1 patient was described previously (Fujikado *et al.*, 2004).

The simulated image using the average value of Zernike coefficients in the triplopia group showed a triple configuration of a Landolt C (*Figure 4*). Although

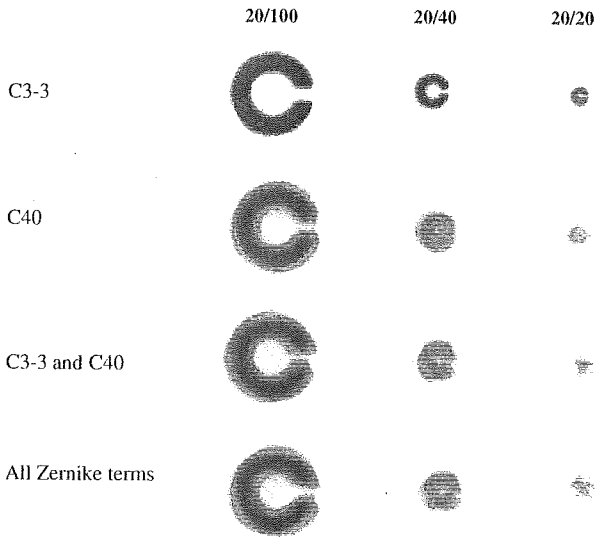

Figure 4. Simulated retinal images of a Landolt C using the average value of Zernike terms in the triplopia group. Neither the trefoil aberration (C3-3) nor the spherical aberration (C40) alone created a triple configuration. But the combination of trefoil and spherical aberration created the triple configuration, which was similar to the simulated image using all of the Zernike terms.

the simulated Landolt' C did not show triplopia when the average values of C3-3 (−0.14 μm) or C40 (−0.21 μm) were used individually, it showed a clear triple configuration if the combination of C3-3 and C40 was used (*Figure 4*).

We also simulated the Landolt C using the value of C33, C42, and the combination of each value with other significantly increased Zernike coefficients in the triplopia group, but the simulated images did not show a triple configuration.

The subjective pinhole test revealed that the triplopia was reduced or disappeared in all eyes.

All nine eyes of six patients underwent cataract surgery. After phacoemulsification and intra-ocular lens implantation, the perceived triplopia disappeared in all eyes. Postoperatively, we measured ocular higher-order aberration in six eyes of four patients (Case 1 R, L, Case 2 R, L, Case 3 R, and Case 4 R) by H-S wavefront sensor. The average value of Zernike term C3-3 changed from −0.14 ± 0.06 μm (preoperative value) to −0.00 ± 0.03 μm (postoperative value) and C40 from −0.21 ± 0.09 to 0.06 ± 0.02 μm. The postoperative values were close to the normal values of the age-matched control group (−0.04 ± 0.05 μm, C3-3 and 0.04 ± 0.01 μm, C40).

Discussion

From the group of patients with cataracts presenting at Osaka University Hospital, a complaint of monocular

triplopia was made by some middle-aged patients with mild nuclear cataract and high myopia. The BCVA of these patients were relatively well-preserved (*Table 1*), and the triplopia was perceived only by middle-aged patients with relatively good visual acuity. This suggests that the age-related cortical cataract, which blurred the retinal image by light scattering, was not increased significantly in these patients (Kuroda *et al.*, 2002b), and the effect of optical aberrations principally contributed to the degradation of the retinal image.

A difference of the Zernike coefficients of the cornea between the triplopia group and control group was observed only in the coma (C3-1) aberration (*Figure 3*). Because the optical aberrations of myopic and emmetropic eyes are not necessarily equivalent (Cheng *et al.*, 2003), the possibility exists that C3-1 is larger in the cornea of myopic eyes.

The significant increase of Zernike terms in the triplopia group, C3-3, C33, C40, and C42 observed in the whole eye, originated in the internal optics of the eye, principally in the lens. This was also supported by the disappearance of the monocular triplopia following removal of the cataract.

Wavefront analysis showed that the triple configuration was caused by the combined increase of the trefoil (C3-3) and spherical aberrations (C40; *Figure 4*). The increase of negative spherical aberration has been reported to be caused by nuclear cataracts (Kuroda *et al.*, 2002c). Nuclear cataracts are observed in highly myopic patients even during middle age (Kaufman and Sugar, 1996). These data suggest that middle-aged patients with high myopia have the potential to develop monocular triplopia if mild nuclear cataracts develop.

The physiological meaning of the increase of trefoil aberration may be the age-related changes of the lambda suture in the lens (Goss *et al.*, 1992b; Kuszak *et al.*, 1994). If the refractive index in the lambda suture area increases with age, the wavefront in these areas is delayed and may cause the trefoil aberration. Triplopia may be perceived if nuclear cataract develops concomitantly with the increase of trefoil aberration (*Figure 5*).

As shown in *Figure 1*, the simulated shape of the triple configuration varies among patients. The shape of the triple configuration may be influenced by other

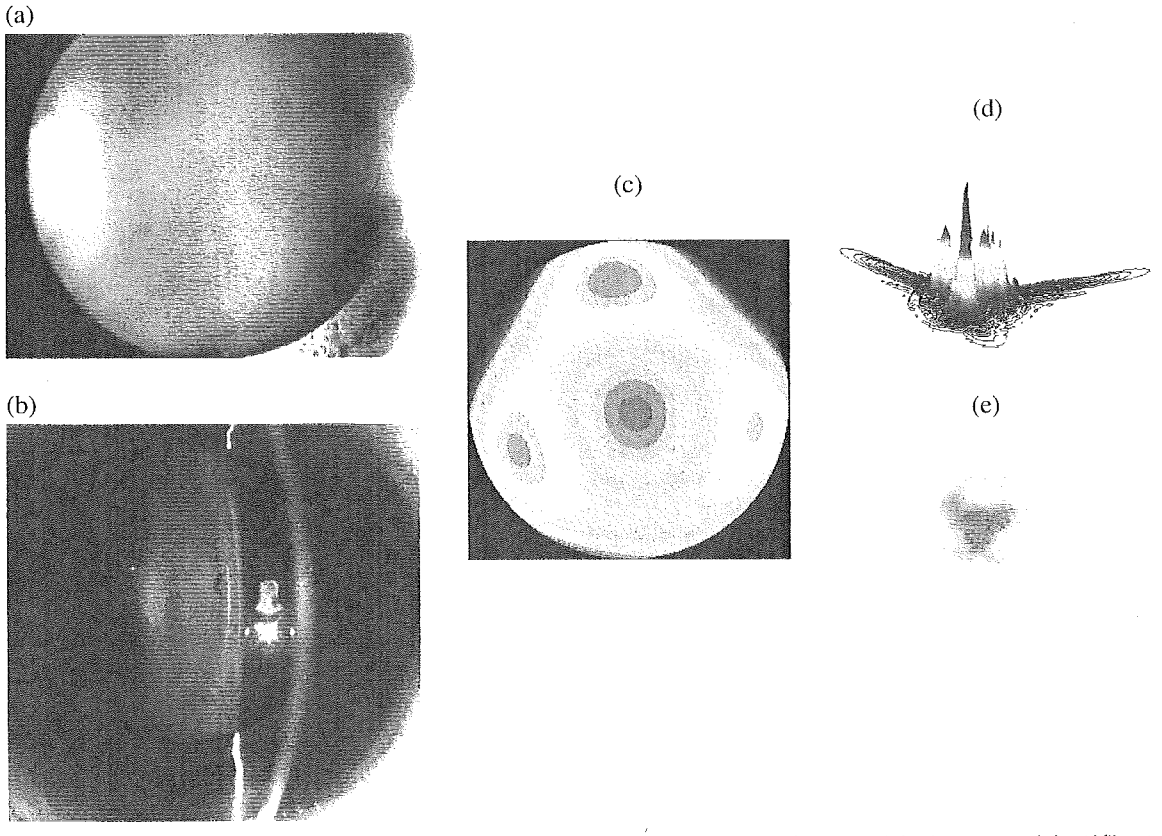

Figure 5. Presumed mechanism of triplopia caused by mild nuclear cataract. The refractive changes of the lens around the "Y" suture area of the lens (a) may cause the trefoil aberration, and the nuclear cataract in the central part (b) causes the negative spherical aberration. The combination of trefoil and negative spherical aberration causes a delayed wavefront in the center and cloverleaf-shaped advanced wavefront in the peripheral pupillary area (c). The PSF obtained from those two Zernike terms shows triple peaks (d), which creates the triple configuration of retinal image (e).